Spectroscopy of narrow, high-lying, low-spin states in ^{20}Ne

J. A. Swartz, B. A. Brown, P. Papka, F. D. Smit, R. Neveling, E. Z. Buthelezi, S. V. Förtsch, M. Freer, Tz. Kokalova, J. P. Mira, F. Nemulodi, J. N. Orce, W. A. Richter, and G. F. Steyn

Phys. Rev. C **91**, 034317 — Published 16 March 2015

DOI: 10.1103/PhysRevC.91.034317

Spectroscopy of narrow, high-lying, low-spin states in ^{20}Ne

J.A. Swartz[1,2], B.A. Brown[3,4], P. Papka[1,2], F.D. Smit[2], R. Neveling[2], E.Z. Buthelezi[2], S.V. Förtsch[2], M. Freer[5], Tz. Kokalova[5], J.P. Mira[1,2], F. Nemulodi[1,2], J.N. Orce[6], W.A. Richter[2,6], G.F. Steyn[2]

[1]*Physics Department, University of Stellenbosch, Private Bag X1, Matieland 7602, South Africa*

[2]*iThemba LABS, P.O. Box 722, Somerset West 7129, South Africa*

[3]*National Superconducting Cyclotron Laboratory, Michigan State University, East Lansing, Michigan 48824, USA*

[4]*Department of Physics and Astronomy, Michigan State University, East Lansing, Michigan 48824, USA*

[5]*School of Physics and Astronomy, University of Birmingham, B15 2TT, UK*

[6]*Physics Department, University of the Western Cape, Private Bag X17, Bellville 7530, South Africa*

(Dated: February 18, 2015)

The excited states of the ^{20}Ne nucleus from the ground state to $E_x = 25$ MeV were investigated with the ^{22}Ne(p,t)^{20}Ne reaction at a beam energy of $E_p = 60$ MeV using the QDD magnetic spectrometer at iThemba LABS. Narrow, low-spin $J^\pi = 0^+$, 1^- and 2^+ states have been observed for the first time at high excitation energies in ^{20}Ne, namely at $E_x = 17.67$, 18.84, 20.59, 21.16, 21.80 and 22.5 MeV. Shell-model and coupled reaction channel calculations were performed to determine the nature of the newly observed states. Candidates for $T = 2$ states are proposed at 3.86(5), 4.43(5) MeV and 5.07(5) MeV above the lowest 0^+, $T = 2$ state at $E_x = 16.73$ MeV. Two of these $T = 2$ candidates appear to result from core-excitations in the $0p$-shell. The state at $E_x = 22.5$ MeV, which could not be interpreted by the shell-model calculations, is a tentative candidate for the 5-α cluster state.

I. INTRODUCTION

At high excitation energies in ^{20}Ne, isobaric analog states (IASs) and α cluster states, which may have low spins and could be narrow, may be anticipated. To date, at least twelve 0^+ and 1^-, and thirteen 2^+ states have been identified at energies up to 18.43 MeV in ^{20}Ne. However, at excitation energies above 18.43 MeV, there are 49 known states in this nucleus [1], most of which have broad widths (usually 100 keV to 500 keV, but some even broader) and none of which have spin values below $J = 4$.

This paper presents results of an experimental study of ^{20}Ne with the ^{22}Ne(p,t)^{20}Ne reaction over a range of reaction angles and energies. The main focus was on small angles including $\theta_{lab} = 0^\circ$ in the region from $E_x = 17$ to 23 MeV, which was investigated for the first time using the (p,t) reaction with high energy-resolution. At forward angles, this reaction provides a high selectivity to low-spin states, hence evidence of 0^+, 1^- and 2^+ states were observed for the first time above $E_x = 20$ MeV in this nucleus. We also provide a theoretical shell-model interpretation for all these states except the highest one at $E_x = 22.5$ MeV, which might be a candidate for the 5-α cluster state.

Two states in ^{20}Ne are known to have isospin $T = 2$ character, the lower, the strong $J^\pi = 0^+$ state at 16.73 MeV [1], is an IAS to the ground state of ^{20}O, and the higher, the 2^+ state at $E_x = 18.43$ MeV [2], is associated with the $E_x = 1.634$ MeV state in ^{20}O [3]. At excitation energies above these two states and their analogs, no evidence of $T = 2$ states have been confirmed in $A = 20$ nuclei [1, 4, 5]. These two states and their known analogs are narrow ($\Gamma \leq 10$ keV) [1, 4], and can be completely described as $1s0d$-shell states [5]. There are also known core-excited states in ^{20}Ne at excitation energies of 7.191 MeV, 12.436 MeV and 13.642 MeV.

Core-excited states may be expected to be more prevalent at higher excitation energies. The state at 12.436 MeV, for example, is a bandhead of $8p$-$4h$ states with a ^{12}C + ^{8}Be cluster structure [6]. In the $A = 20$ nuclei ^{20}O, ^{20}F and ^{20}Ne, core-excited $T = 2$ states may be anticipated as positive parity states with $6p$-$2h$ configurations, or as negative parity states with $5p$-$1h$ configurations. Notably, the 0^+ state at 4.456 MeV in ^{20}O has long been known to have a $6p$-$2h$ configuration [7], and its IAS state may be expected above 20 MeV in ^{20}Ne.

The structure of ^{20}Ne at equilibrium is that of a prolate, axially symmetric quadrupole ellipsoid [8]. As opposed to the single-particle level degeneracy found in spherical nuclei, this deformation causes degeneracy around shell closures creating conditions that are favorable for clustering [9], which shell-model calculations have trouble reproducing [10]. For this reason cluster models are often used to describe bands of states around such shell closures while core-cluster calculations fare better even for light nuclei [11, 12].

Microscopic calculations with Antisymmetrized Molecular Dynamics (AMD) [10, 13] and Fermionic Molecular Dynamics (FMD) [14] have been particularly successful in reproducing clustering in light nuclei. Given its deformation and many excited states prone to α-decay, ^{20}Ne is an ideal example of clustering in nuclear matter [15]. The theories of Morinaga and Ikeda predict that a 0^+ 5-α 'Hoyle-like' cluster state may exist in the region near the 5-α breakup threshold of ^{20}Ne at $E_x = 19.17$ MeV [16]. The observation of low-spin states in this region may provide meaningful information towards the identification of such a state.

II. THE EXPERIMENT

A 60 MeV dispersion matched [17] proton beam was provided by the Separated Sector Cyclotron (SSC) at iThemba LABS, Cape Town, South Africa. The beam, which varied in intensity from 1 to 20 nA, impinged upon a ^{22}Ne gas cell target. The triton ejectiles were focused by the magnets of the K600 QDD magnetic spectrometer [18] onto the focal plane detectors. Measurements were performed for a range of ejectile laboratory angles. For the forward scattering angles, including $\theta_{lab} = 0°$, the spectrometer was positioned at angles varying from $\theta_{lab} = 0.5°$ to $\theta_{lab} = -1°$. A specific combination of spectrometer field setting and angle was selected to minimize the background, since the beam was stopped in a Faraday cup inside the first dipole magnet of the spectrometer. However, the $\pm$ 2° angular acceptance of the spectrometer ensured that $\theta_{lab} = 0°$ was included in all these measurements. For measurements at the larger laboratory angles θ_{lab} = (7°, 16°, 27°), the beam was stopped in a Faraday cup inside the scattering chamber.

The focal plane detectors consisted of two multi-wire drift chambers, followed by a plastic scintillation detector. This scintillator provides the trigger signal and also aids with particle identification by providing energy loss and time-of-flight (TOF) information. The TOF information was generated by the time difference between scintillator signals and the RF signal for the pulsed beam.

At 60 MeV, the time interval between separate beam packets from the cyclotron is only 41 ns. This is much less than the anticipated flight time of the tritons and deuterons, which were the two particle species from which significant count rates could be expected, based on magnetic rigidity calculations. Therefore, pulse selection of one in every five beam packets was employed, thus stretching the interval between packets to 205 ns. This was long enough to ensure clear separation between tritons and deuterons. Fig. 1 shows a particle identification spectrum, measured at θ_{lab} = -1°, where prominent loci were identified that represent the tritons, deuterons and also a significant background related to the K600 internal beam stop.

The gas cell target was designed for a wide dispersive beam, and can accommodate a greater range of reaction angles in the horizontal than in the vertical direction. Its 10 mm thick aluminium body has an opening which is 30 mm wide and 10 mm high. The entrance and exit windows of the gas target consisted of 6 μm thick aramid foils spaced 10 mm apart. The chemical composition of the aramid material is $C_{14}O_2N_2Cl_2H_8$ with associated weight ratios (C, O, N, Cl, H) = 54.74, 10.42, 9.12, 23.09, 2.63 [19, 20], hence considerable contamination from these elements in the foils could be anticipated in the data obtained with the neon gas. The gas target cell was filled to pressures of approximately P = 1.5 bar.

The ^{22}Ne gas that was used in this experiment is reported to be 99.97% isotopically pure [21]. Measurements were performed with a residual gas analyzer to determine the strengths of contaminants in the gas. The only noticeable contamination was from xenon isotopes, at partial pressures of five orders of magnitude below that of the ^{22}Ne gas. From Q-value calculations, it was found that none of the xenon isotopes could interfere in the main excitation energy region of interest (E_x = 17 to 23 MeV).

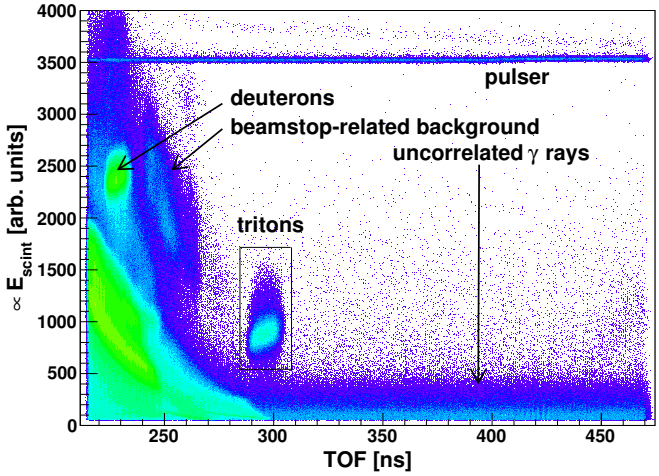

FIG. 1. (Color online) A particle identification spectrum, measured with a magnetic field setting for E_x = 17 to 23 MeV for the ^{22}Ne(p,t) reaction and a spectrometer angle of θ_{lab} = -1°.

III. ANALYSIS AND RESULTS

Making use of a gas cell, with its extended size as a target, as opposed to the normal thin foils has its own challenges. In spectra measured with a gas-filled target, background peaks originating from the aramid foils appeared as double peaks. This effect is caused by the difference in energy loss between tritons and protons through the gas in the cell as the (p,t) reaction can occur on either the entrance or the exit foil.

Known states in ^{20}Ne were used for calibration purposes in the low excitation energy field sets. A reliable calibration for the high excitation energy region was obtained from the ^{16}O(p,t)^{14}O reaction as measured with natural oxygen gas, since the energy loss of tritons through the oxygen gas in the gas cell mimicks the energy loss of tritons through neon. To further investigate the sources of experimental background, in-beam investigations on foils of carbon and aramid were performed as well as with the target gas cell filled with natural oxygen, nitrogen, neon and argon. Superimposed spectra, measured with the oxygen gas cell for the highest excitation energy field setting (E_x = 17 to 23 MeV) at θ_{lab} = -1°, along with results for a ^{12}C foil and a single aramid foil, are shown in Fig. 2.

To correct for double peaked background from the aramid foils, a spectrum from a single aramid foil was plotted twice, as shown in Fig. 3, with a small shift between the spectra. The size of the shift was determined

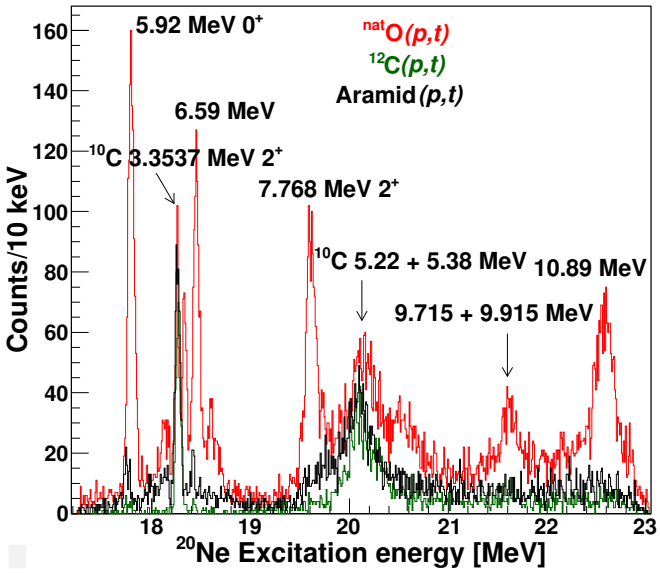

FIG. 2. (Color online) Excitation energy spectra in the excitation energy region E_x = 17 to 23 MeV for the ^{22}Ne(p,t)^{20}Ne reaction at θ_{lab} = -1° for the natural oxygen target as well as ^{12}C and aramid foils.

from the energy difference between the double peaks observed in the spectra measured with the ^{22}Ne gas-filled cell. This was then subtracted from the data acquired with the ^{22}Ne filled gas target.

The data obtained for the ^{22}Ne gas-filled target at different magnetic field settings, covering an excitation energy range from the ground state to 23 MeV, are shown for angles near $\theta_{lab} = 0°$ in Fig. 4. States identified to be populated by the (p,t) reaction on the aramid foil [22] are indicated by the peaks which are colored in red in Fig. 4. The six states at E$_x$ = 17.67 MeV, 18.84 MeV, 20.59 MeV, 21.16 MeV, 21.80 MeV and 22.5 MeV, colored in blue, were not known prior to this study. The energy uncertainty of peak positions in ^{20}Ne was estimated to be ± 50 keV, and the resolution of the measurement varied around 40 keV.

The cross sections which were extracted for all states that were known prior to this study are shown in Table I, while the new ones are shown in Table II. Most of these states were observed near 0° while many were seen also, and in some cases only, at larger angles. Each of the newly measured states were observed at very forward angles that include $\theta_{lab} = 0°$, as well as at least one other angle.

The new state at $E_x = 21.16$ MeV is a 0^+ state, from its angular distribution spectrum which is shown in Fig. 5. Spin and parities can not be unambiguously assigned to the new states at 17.67, 18.84, 20.59 and 21.80 MeV, but the angular distributions of these states indicate 2^+, $0^+/1^-$, $1^-/2^+$ and $0^+/1^-$ respectively, as possible assignments.

The state at $E_x = 22.5$ MeV is unfortunately situated on a background consisting of the $E_x = 10.89$ MeV state

TABLE I. Extracted cross sections for the known states which were observed in ^{20}Ne. *NI* indicates that the energy region around a state was not investigated at a particular angle. Known excitation energies and J^π values taken from Ref. [1].

E_x MeV	J^π	σ(-1°) [μb sr^{-1}]	σ(7°) [μb sr^{-1}]	σ(16°) [μb sr^{-1}]	σ(27°) [μb sr^{-1}]
g.s.	0^+	620(140)	670(150)	160(36)	160(35)
1.634	2^+	250(56)	250(57)	58(13)	40(9)
4.428	4^+	110(24)	150(33)	120(27)	120(26)
5.621	3^-	34(7)	104(23)		*NI*
5.788	1^-	50(11)	48(11)		*NI*
6.725	0^+	110(24)		12.0(25)	*NI*
7.191	0^+	77(17)	27(6)	24(5)	*NI*
7.421	2^+	93(21)	21(5)		*NI*
7.833	2^+	7.7(17)	19(4)	18(4)	*NI*
9.031	4^+	12.0(27)		9(2)	*NI*
9.487	2^+	5.7(13)	17(4)	66(15)	*NI*
9.873	3^-			3.3(7)	*NI*
9.9	4^+	2.3(5)			*NI*
10.273	2^+	35(8)	160(36)	280(63)	*NI*
10.406	3^-	5.8(13)		3.3(8)	*NI*
10.553, 10.584	4^+, 2^+	3.1(7)	8(2)	26.0(58)	*NI*
10.84, 10.843	3^-, 2^+	16.0(35)	49(11)	45(10)	*NI*
11.09	4^+	58(13)	77(17)	81(18)	*NI*
11.32	0^+		5.8(13)		*NI*
11.528, 11.555, 11.558	3^-, 4^+, 3^+, 0^+	22(5)	21(5)	19(4)	*NI*
12.221	2^+	61(14)	120(26)	190(41)	*NI*
12.401, 12.436	3^- 0^+	7.6(17)	12.0(27)	12.0(26)	*NI*
12.743	(2^+)	23(5)	15.0(34)		*NI*
13.048	4^+	46(10)	61(14)	77(17)	*NI*
13.642	0^+	57(13)	42(9)		*NI*
13.744	0^+	28(6)	59(13)		*NI*
13.827, 13.866	3^-, 1^-	3.2(7)		2.7(6)	*NI*
14.063, 14.115	2^+, 2^+		18(4)		*NI*
14.370				23(5)	*NI*
14.455, 14.475	$(0^+,2^+)$, 0^+	50(11)	52(11)	18(4)	*NI*
14.653	0^+	24.0(69)			*NI*
14.839, 14.888	(4^+), 2^+	11.0(25)	16.0(35)	39.0(87)	*NI*
15.436, 15.500	(3^-),	16.0(36)			*NI*
16.73	0^+	370(82)	186(42)	35(8)	65(15)
17.155	5^-			3.2(7)	
17.284	3^-			4.6(10)	2.7(6)
17.541, 17.55	6^+, (2^+)			11(2)	
17.91	(2^+)	3.2(7)		14(3)	13(3)
18.286	6^+				4.1(9)
18.43	2^+	29(7)		10(2)	14(3)
19.443	6^+				20(4)
20.296	7^-				5.0(11)

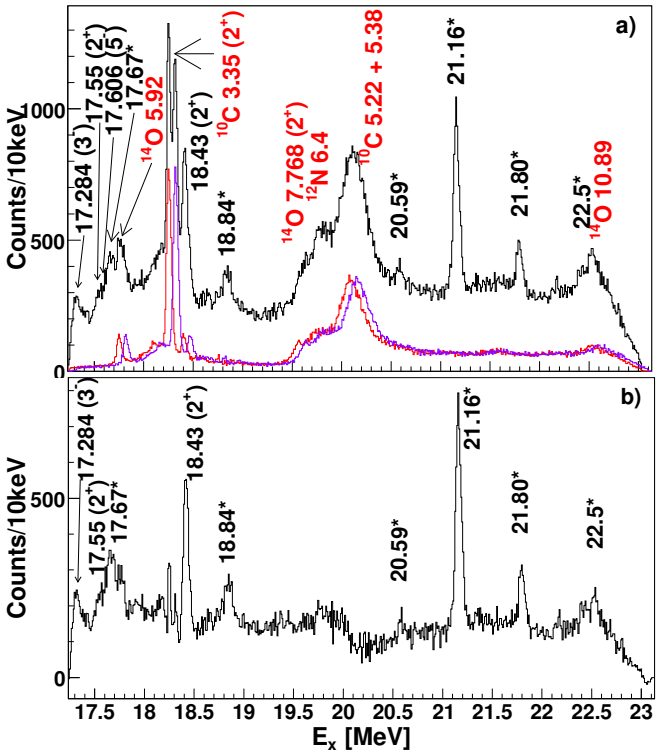

FIG. 3. (Color online) Excitation energy spectrum for the ^{22}Ne gas target in the excitation energy region 17-23 MeV at θ_{lab} = -1° (black spectrum), compared to charge normalized background data measured with a single aramid foil (red and purple spectra) in a). The background subtracted ^{22}Ne(p,t)^{20}Ne spectrum is shown in b).

of ^{14}O from the ^{16}O(p,t)^{14}O reaction on the aramid foil. Fig. 3 shows the data obtained for ^{22}Ne in the excitation energy region 17-23 MeV at θ_{lab} = -1° before and after subtraction of the charge-normalized background data. It is clear that some strength is still present in this state at θ_{lab} = -1°. This state also retains some strength after background subtraction at θ_{lab} = 7°, while at θ_{lab} = 16° and θ_{lab} = 27° it was beyond the energy region of focal plane coverage by the spectrometer. Its cross section could be extracted, though with large uncertainties as shown in Fig. 5, at θ_{lab} = -1° and θ_{lab} = 7° [22]. Its angular distribution is consistent with a 0$^+$ state.

IV. DISCUSSION

The possible theoretical partners of the six newly observed states are indicated in Table II and Fig. 5. For the candidate theoretical partners of the 17.67 MeV and 18.84 MeV states, the results are model dependent. Therefore, some states generated with a USDA Hamiltonian [23] are indicated by a in Table II, while ones from USDB are indicated by b [23].

Fig. 6 shows cross sections for 0$^+$ states determined from the experiment and calculations. Regions of excitation that are affected by contaminants in the experiment are indicated by the horizontal red lines. The three lower panels show the direct-reaction cross sections obtained from two-particle transfer amplitudes from the 1s0d-shell USD, USDB and USDA Hamiltonians [23]. We use the reaction code FRESCO [24, 25] with the Bechetti-Greenless optical model parameters for protons [26] and tritons [27]. All theoretical cross sections are multiplied by a factor of three to obtain an overall agreement with experiment. This factor may be needed to account for sequential transfer as well as deficiencies in the optical potentials. The three 1s0d Hamiltonians all give similar results. Other than the ground state (not shown) the largest cross section is for the T = 2 state near E_x = 17 MeV labeled by "2" in the figure. It corresponds to the well known experimental T = 2 state at E_x = 16.73 MeV labeled by "2" in the top panel (see Table III).

The first 2$^+$, T = 2 state at 18.43 MeV is also well known (Table III). The second 2$^+$, T = 2 state, which is predicted at E_x = 20.81 MeV and has an IAS at E_x = 4.072 MeV in ^{20}O, may be related to the 20.59(5) MeV state from the data as suggested in Table II. In the 1s0d-shell theory, only one 0$^+$ state is predicted near E_x = 7 MeV. We calculated $2\hbar\omega$ wavefunctions with the WBP Hamiltonian [28] in the $0s-0p-0s1d-0f1p$ model space. The structure calculations were carried out with the OXBASH [29] code. The cross sections obtained for these states, which are also multiplied by a factor of three as are all the theoretical cross sections, are shown by the red peaks in Fig. 6 in the same panel as the USD results. The structure of the $2\hbar\omega$ wavefunctions is dominated by the excitation of two

TABLE II. Extracted cross sections and natural widths for the six new states in ^{20}Ne. States generated by OXBASH are bold-faced and accompanied by angular distributions generated by FRESCO. The experimental states are not bold-faced. The symbol a denotes states calculated with the USDA Hamiltonian, while b denotes states calculated with the USDB Hamiltonian.

E_x MeV	σ(-1°) [μb sr^{-1}]	σ(7°) [μb sr^{-1}]	σ(16°) [μb sr^{-1}]	σ(27°) [μb sr^{-1}]	Γ [keV]
17.670(57)	2.2(5)	7.3(21)	10.0(25)	7.7(20)	114(48)
a **17.350 2$^+$**	3.3	4.8	7.5	4.8	
b **18.020 2$^+$**	2.6	3.6	5.7	3.6	
18.840(56)	12(3)		6.7(15)		97(41)
a **19.020 0$^+$**	50.1	28.2	10.3	18.0	
b **19.270 0$^+$**	26.1	14.7	5.7	9.6	
18.630 1$^-$	14.1	24.3	21.3	11.1	
18.970 1$^-$	7.5	14.6	11.4	6.0	
20.590(54)	2.4(5)	6.7(15)			$\leq$ 55
20.810 2$^+$	2.1	2.4	2.7	1.8	
21.160(53)	38(9)	22(5)	7.2(16)	7.7(17)	$\leq$ 43
20.470 0$^+$	61	33	4.5	10.8	
21.800(53)	11.0(26)	7.3(16)			$\leq$ 38
21.720 1$^-$	2.7	6.6	7.2	3.9	
22.500(52)	22.0(49)	11.0(52)			260(52)

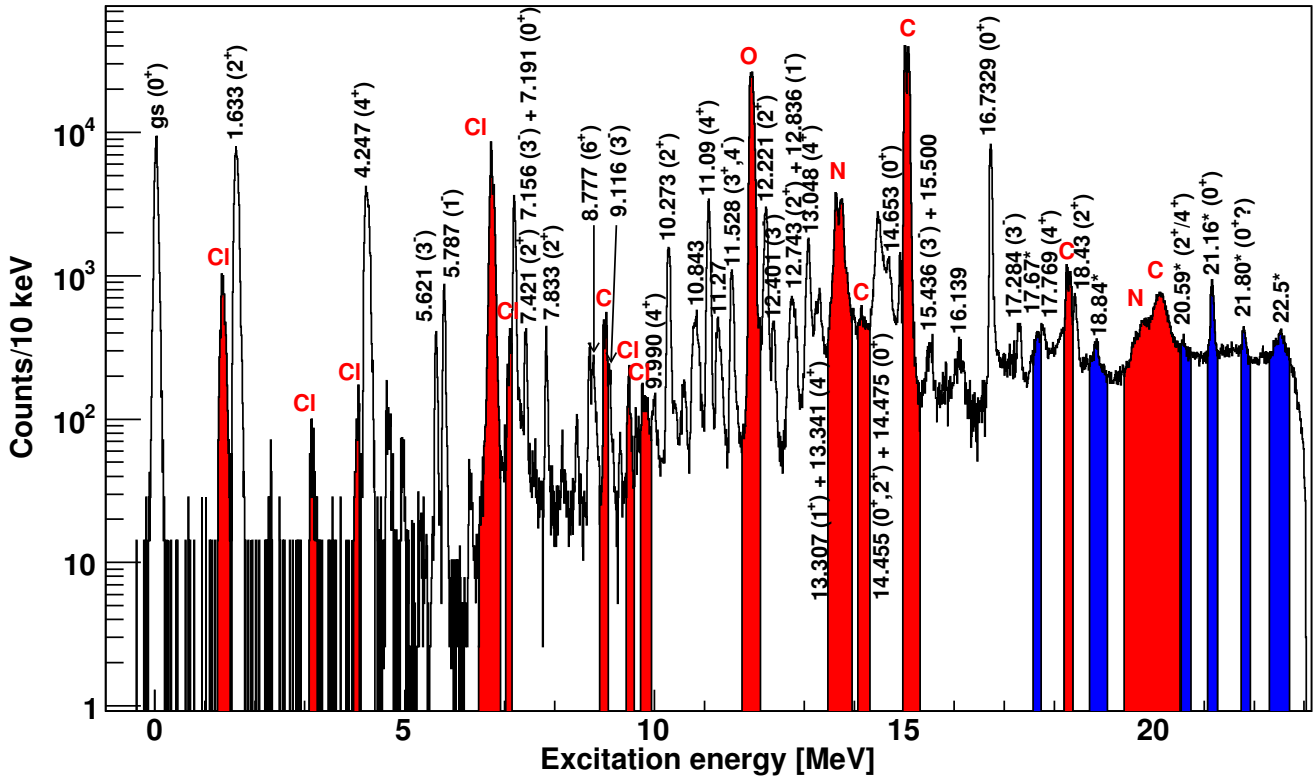

FIG. 4. (Color online) The excitation energy spectrum for the ^{22}Ne(p,t)^{20}Ne reaction at 60 MeV measured at angles close to $\theta_{lab} = 0°$. New states are indicated by a black asterisk and colored in blue. The data were obtained at five different magnetic field settings, each normalized in total charge to the field setting for the E_x = 17 - 23 MeV range, which is where the most statistics were accumulated.

holes from the $0p$ shell to the $1s0d$ shell. These states can be populated in the ^{22}Ne(p,t) reaction by the removal of two neutrons from the $0p$ shell. We find a significant cross section for some $2\hbar\omega$ states. In particular, another state near 7 MeV appears. This is the lowest energy "intruder" relative to the $1s0d$ model space. The strongest $2\hbar\omega$ state is a $T = 1$ state near 12.5 MeV labeled by "1" in the figure. It corresponds to the experimental $T = 1$ state at 13.642 MeV that is 3.351 MeV above the well known 2^+, $T = 1$ state at 10.273 MeV. The experimental isobaric analog of this state in ^{20}F is at an excitation energy of 3.526 MeV above the 2^+ ground state. The theoretical strength for this state may be fragmented among other $T = 1$ or $T = 0$ states in this region of excitation energy (the fragmentation with $T = 0$ would be due to isospin mixing). Also some of the strength may be missed experimentally due to the regions affected by contamination. The $2\hbar\omega$ spectrum also contains a relatively strong 0^+, $T = 2$ state at 20.47 MeV (indicated by the red label "2" in the figure) that is 3.810 MeV above the lowest theoretical $T = 2$ state. This state is most likely associated with the experimental state at 21.16(5) MeV that is 4.43(5) MeV above the lowest 0^+, $T = 2$ state at 16.73 MeV. The isobaric analog of this $T = 2$ intruder state is known at 4.456 MeV in ^{20}O [7]. The Q value for allowed proton decay to the $1/2^+$ state at 7.364 MeV in ^{19}F is 20.19 MeV, and the $l = 0$ proton single-particle decay width for a state that is unbound by one MeV is about 150 keV. Since the proposed state at 21.16 MeV has an intruder configuration its spectroscopic factor will be small with a resulting width consistent with the experimental upper limit of $\Gamma = 43$ keV.

Negative parity states arise in the $s-p-sd-pf$ model space from $1\hbar\omega$ excitations. The cross sections calculated for the 1^- states have angular distributions that are flat from 0° to 10° and must be considered for the small angle spectra. Above 17 MeV, the only strong 1^- state from the theory is the $T = 2$ state in Table II at 21.72 MeV (the lowest negative parity $T = 2$ state). Its cross section is within a factor of four of the observed state at 21.80 MeV (5.07 MeV above the 0^+, $T = 2$ state). The calculated allowed $l = 1$ decay width of this state is less than $\Gamma = 1$ keV. This is consistent with the experimental upper limit of $\Gamma = 38$ keV which was measured for the state at 21.80 MeV. A candidate for the isobaric analog of this state in ^{20}O is the state at $E_x = 5.115$ MeV with an unassigned spin [30].

All the $T = 2$ states in the isobars ^{20}Ne, ^{20}F and ^{20}O, including the three newly measured candidate $T = 2$ states in ^{20}Ne, are shown in Table III, with IAS partners indicated on the same line. Fig. 7 shows a diagram for $T = 1$ and $T = 2$ IAS states in these three nuclei,

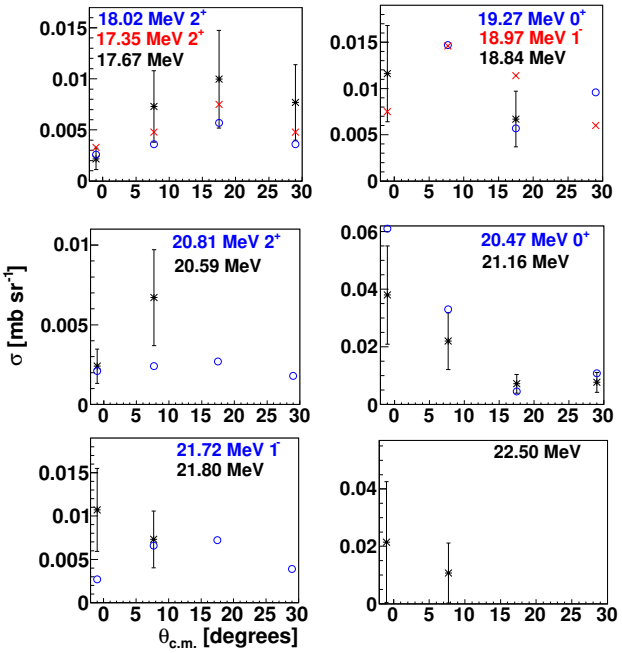

FIG. 5. (Color online) Comparison of experimental and theoretical ^{22}Ne(p,t)^{20}Ne cross sections for new states shown in Table II. Values and angular distributions of measured states are indicated in black, while the angular distribution calculated with FRESCO is shown, for each state, in the same color as is used for the value calculated with OXBASH, which is indicated in each panel above the measured value.

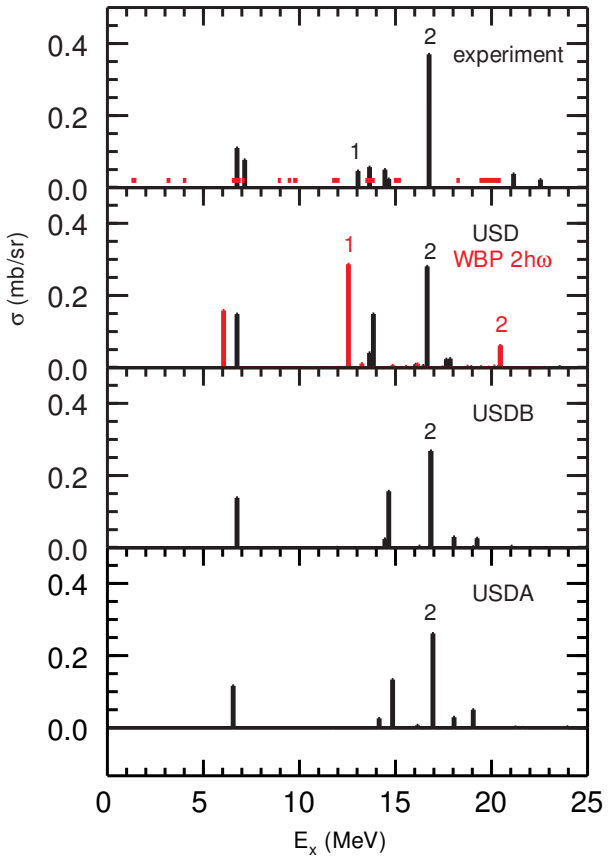

FIG. 6. (Color online) Comparison of experimental and theoretical ^{22}Ne(p,t)^{20}Ne cross sections for 0^+ states. Details are discussed in the text.

TABLE III. States with $T = 2$ isospin in ^{20}Ne, and their IAS partners in ^{20}F and ^{20}O. The $T = 2$ candidates measured in the present experiment are bold-faced. The model space used to describe each state, and the energies which were calculated for each new state using these model spaces, are shown in the second column.

^{20}Ne E_x MeV	^{20}Ne E_x (theory) [MeV]	^{20}F E_x [MeV]	^{20}O E_x [MeV]
16.73 0^+	$0\hbar\omega$	6.519 0^+	g.s. 0^+
18.43 2^+	$0\hbar\omega$	8.500	1.673 2^+
(20.59 2^+)	20.81 $0\hbar\omega$		4.072 2^+
(21.16 0^+)	20.47 $2\hbar\omega$		4.456 0^+
(21.80 1^-)	21.72 $1\hbar\omega$		5.115

based on the new IAS candidates in ^{20}Ne. The highest three states of ^{20}Ne are the candidate $T = 2$ states and the highest three in ^{20}O are their IAS partner candidates. These correspond to the bottom three states of the respective nuclei in Table III.

The theory described above accounts for all narrow states at small angles in (p,t) up to $E_x = 21.8$ MeV. Above this we find one more state which is consistent with a 0^+ character at 22.5 MeV that cannot be accounted for in the $1s0d$, $2\hbar\omega$ or $1\hbar\omega$ model spaces. This is not likely to be a $T = 2$ state since the above calculations account for all the observed $T = 2$ states in ^{20}O below 6 MeV. We may speculate that this is the 5-α cluster state. The energy of this state is predicted to be 22.14 MeV, based on the Hill-Wheeler equation applied to a 5-α condensate model [31]. It could be narrow because of its unique cluster structure. We cannot calculate the theoretical cross section for this, but note the 3-α state in ^{12}C is observed in ^{14}C(p,t) with a strength of 3.5% of the ground state at a beam energy of 40 MeV [32]. In the current experiment, the 22.5 MeV state was measured with a strength of 3.5% and 1.6% of that of the ground state of ^{20}Ne at $\theta_{lab} = -1°$ and $\theta_{lab} = 7°$ respectively [22], which shows good agreement with the ^{14}C(p,t) result.

Table IV shows a list of 0^+ states measured in the present experiment, compared to the ones which were predicted by the calculations with OXBASH and the 5-α condensate model.

V. CONCLUSION AND OUTLOOK

In summary, a measurement of the ^{22}Ne(p,t)^{20}Ne reaction was performed to investigate ^{20}Ne particularly in

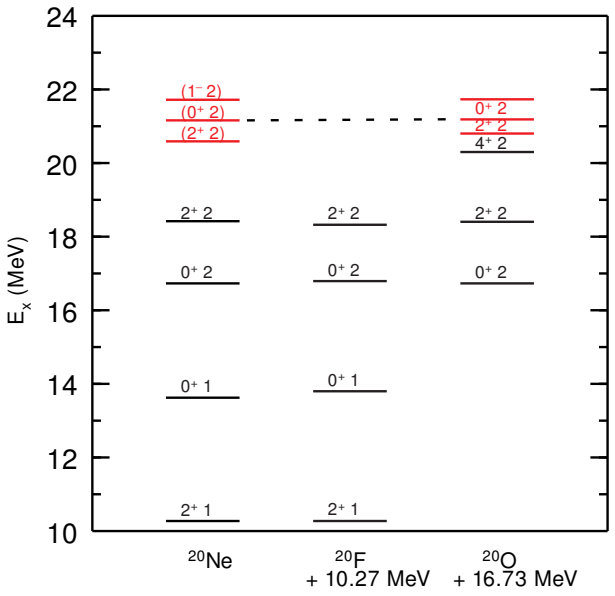

FIG. 7. (Color online) $T = 1$ and $T = 2$ states at excitation energies above 10 MeV in ^{20}Ne and their known isobaric analog states in ^{20}Ne, ^{20}F and ^{20}O, incorporating the newly measured states, indicated in red as are their proposed partners, from the present measurement.

TABLE IV. States with 0^+ character predicted by OXBASH, compared to 0^+ states measured in experiment.

E_x Calculated MeV	Model	E_x Measured [MeV]
6.05	$2\hbar\omega$	6.725
6.70	USDB	7.191
12.58	$2\hbar\omega$	13.642
14.43	USDB	14.455/14.475
14.67	USDB	14.653
16.76	USDB	16.73
18.06	USDB	17.90
19.02	USDB	18.840(56)
20.47	$2\hbar\omega$	21.160(53)
22.14	5-α [31]	22.500(52)

the excitation energy region $E_x = 17$ - 23 MeV, and six narrow states with low spin values ($J = 0$ - 2) were discovered. All of these states are accounted for within the $1s0d$, $2\hbar\omega$ or $1\hbar\omega$ model spaces, apart from the one at $E_x = 22.5$ MeV, which may possibly be the first 5-α cluster state in ^{20}Ne. Three of these states appear to have $T = 2$ isospins at $E_x > 20$ MeV. This signifies the first indication of $T = 2$ states in $A = 20$ nuclei at excitation energies above the state at 18.43 MeV in ^{20}Ne and its analogs. Only one of these $T = 2$ states, at $E_x = 20.59$ MeV, could be described as a $1s0d$ state. Calculations performed within the $2\hbar\omega$ and $1\hbar\omega$ model spaces indicate that the states at $E_x = 21.16$ MeV and 21.80 MeV respectively may be assigned to core excitations from the $0p$-shell with $6p$-$2h$ and $5p$-$1h$ configurations.

A coincident measurement with cleaner background conditions will be necessary to identify the 5-α cluster state and to ascertain the nature of some of the newly observed states from this experiment. The 5-α cluster candidate at $E_x = 22.5$ MeV needs to be investigated for α-decay specifically to search for an α-cluster character. The states at 20.59 MeV, 21.16 MeV and 21.80 MeV may be expected to undergo proton-decay with energies smaller than 2 MeV owing to the high Q value for allowed proton decay from $T = 2$ states (20.19 MeV).

ACKNOWLEDGMENTS

The financial assistance of the South African National Research Foundation (NRF) towards this research is hereby acknowledged. The authors thank Atsushi Tamii for providing the aramid foils for the gas target, Carlos Pineda-Vargas and Christopher Mtshali for performing an ion beam analysis on these foils, and the accelerator team at iThemba LABS for providing a high quality beam. We acknowledge support from NSF grant PHY-1404442.

[1] Experimental Nuclear Reaction Data Library (EXFOR), IAEA Nuclear Data Section. See: http://www-nds.iaea.org/exfor/ or, for the NNDC at Brookhaven National Laboratory, the mirror site is http://www.nndc.bnl.gov/exfor/.

[2] W. N. Catford, E. F. Garman, and L. K. Fifield, Nucl. Phys. A **417**, 77 (1984).

[3] J. Cerny, R. H. Pehl, and G. T. Garvey, Phys. Lett. **12**, 234 (1964).

[4] A. Gade *et al.*, Phys. Rev. C **76**, 024317 (2007).

[5] H. T. Fortune, R. Sherr, and B. A. Brown, Phys. Rev. C **85**, 054304 (2012).

[6] M. M. Hindi, J. H. Thomas, D. C. Radford, and P. D. Parker, Phys. Rev. C **27**, 2902 (1983).

[7] S. LaFrance, H. T. Fortune, S. Mordechai, M. E. Cobern, G. E. Moore, R. Middleton, W. Chung, and B. H. Wildenthal, Phys. Rev. C **20**, 1673 (1979).

[8] R. H. Spear, Phys. Rep. 73, 369 (1981).

[9] J. P. Ebran, E. Khan, T. Niksic, and D. Vretenar, Letters to Nature **487**, 341 (2012).

[10] H. Horiuchi, K. Ikeda, and K. Kato, Prog. Theor. Phys. Supplement No. 192 (2012).

[11] B. Buck, A. C. Merchant, and S. M. Perez, Phys. Rev. C **87**, 024304 (2013).

[12] B. Buck, C. Dover, and J. P. Vary, Phys. Rev. C **11**, 1803 (1975).

[13] Y. Kanada-Enyo, and H. Horiuchi, Prog. Theor. Phys. 142 (Suppl.), 205263 (2001).

[14] T. Neff, and H. Feldmeier, Int. J. Mod. Phys. E17, 2005 (2008).

[15] M. Freer, *Reports on Progress in Physics* **70** 2149 (2007).

[16] K. Ikeda, N. Takigawa, and H. Horiuchi, Suppl. Prog. Theor. Phys. **Extra Number**, 464 (1968).

[17] H. Fujita *et al.*, Nucl. Instr. Meth. A **484**, 17 (2002).

[18] R. Neveling *et al.*, Nucl. Instr. Meth. A **654**, 29 (2011).

[19] Toray Group, www.toray.com, (2013).

[20] A. Tamii, Private communication.

[21] Chemgas, http://www.chemgas.com, (2013).

[22] J. A. Swartz, PhD thesis, Stellenbosch University, scholar.sun.ac.za/handle/10019.1/86443 (2014).

[23] B. A. Brown and W. A. Richter, Phys. Rev. C **74**, 034315 (2006).

[24] The FRESCO website, www.fresco.org.uk, (2006).

[25] I. J. Thompson, Computer Physics Reports **7**, 167 (1988).

[26] F. D. Bechetti and G. W. Greenlees, Phys. Rev. **182**, 1190 (1969).

[27] F. D. Bechetti and G. W. Greenlees, At. Data Nucl. Data Tables, **17**, 6 (1976).

[28] E. K. Warburton and B. A. Brown, Phys. Rev. C **46**, 923 (1992).

[29] B. A. Brown, E. Etchegoyen, W. D. M. Rae and N. S. Godwin, OXBASH, 1984 (unpublished).

[30] M. Wiedeking *et al.*, Phys. Rev. Lett. **94**, 132501 (2005).

[31] T. Yamada and P. Schuck, Phys. Rev. C **69**, 024309 (2004).

[32] M. Yasue *et al.*, Nucl. Phys. A **510**, 285 (1990).